Cell Tissue Res (2012) 347:603–612
DOI 10.1007/s00441-011-1298-z

REVIEW

Biomimetic tubular nanofiber mesh and platelet rich plasma-mediated delivery of BMP-7 for large bone defect regeneration

A. Berner · J. D. Boerckel · S. Saifzadeh · R. Steck · J. Ren · C. Vaquette · J. Qiyi Zhang · M. Nerlich · R. E. Guldberg · D. W. Hutmacher · M. A. Woodruff

Received: 26 September 2011 / Accepted: 7 December 2011 / Published online: 26 January 2012

Abstract There is a growing need for successful bone tissue engineering strategies and advanced biomaterials that mimic the structure and function of native tissues carry great promise. Successful bone repair approaches may include an osteoconductive scaffold, osteoinductive growth factors, cells with an osteogenic potential and capacity for graft vascularisation. To increase osteoinductivity of biomaterials, the local combination and delivery of growth factors has been developed. In the present study we investigated the osteogenic effects of calcium phosphate (CaP)-coated nanofiber mesh tube-mediated delivery of BMP-7 from a PRP matrix for the regeneration of critical sized segmental bone defects in a small animal model. Bilateral full-thickness diaphyseal segmental defects were created in twelve male Lewis rats and nanofiber mesh tubes were placed around the defect. Defects received either treatment with a CaP-coated nanofiber mesh tube (n=6), an un-coated nanofiber mesh tube (n=6) a CaP-coated nanofiber mesh tube with PRP (n=6) or a CaP-coated nanofiber mesh tube in combination with 5 μg BMP-7 and PRP (n=6). After 12 weeks, bone volume and biomechanical properties were evaluated using radiography, microCT, biomechanical testing and histology. The results demonstrated significantly higher biomechanical properties and bone volume for the BMP group compared to the control groups. These results were supported by the histological evaluations, where BMP group showed the highest rate of bone regeneration within the defect. In conclusion, BMP-7 delivery via PRP enhanced functional bone defect regeneration, and together these data support the use of BMP-7 in the treatment of critical sized defects.

Keywords Bone defect · Bone tissue engineering · Growth factors · Bone morphogenetic protein · Nanofiber mesh

A. Berner and J. D. Boerckel: these authors contributed equally to this work

Electronic supplementary material The online version of this article (doi:10.1007/s00441-011-1298-z) contains supplementary material, which is available to authorized users.

A. Berner · S. Saifzadeh · R. Steck · J. Ren · C. Vaquette · J. Q. Zhang · D. W. Hutmacher · M. A. Woodruff (✉)
Institute of Health & Biomedical Innovation,
Queensland University of Technology,
60 Musk Avenue, Kelvin Grove,
4059 Brisbane, Queensland, Australia
e-mail: mia.woodruff@qut.edu.au

A. Berner · M. Nerlich
Department of Trauma Surgery, University of Regensburg,
Regensburg, Germany

J. D. Boerckel · R. E. Guldberg · D. W. Hutmacher
School of Mechanical Engineering,
Parker H. Petit Institute for Bioengineering and Bioscience,
Georgia Institute of Technology,
Atlanta, USA

Introduction

Bone is a dynamic and multifunctional organ, with remarkable capacity for self-repair. However, in certain cases, where healing and repair functions are impaired, surgical therapeutic intervention is required due to a limited intrinsic regeneration potential (Perry 1999). For challenging cases, such as open fractures and large bone defects, tissue engineering has emerged as a promising approach to bone regeneration. For these situations, important considerations include an osteoconductive scaffold, growth factors, vascularisation of the graft and supply of cells with osteogenic potential.

The development of appropriate biomaterials for tissue regeneration has become a key research drive in bone tissue engineering. Most biomaterials suffer from limited bioactivity and therefore must be used in combination with osteoinductive supplements. One of the most frequently used techniques for overcoming lack of osteoinductivity is the local delivery of growth factors, such as members of the bone morphogenetic protein (BMP) family, vascular endothelial growth factors (VEGF) and transforming growth factor- ß (TGF-ß) (Xiao et al. 2011).

Among these growth factors, BMPs have been shown to play an important role in osteogenic differentiation. In 1965, Urist's discovery of the osteoinductive capacity of the demineralised bone matrix brought attention to the role of growth factors found within the matrix (Urist 1965). Subsequently, more than 15 osteogenic proteins or BMPs have been discovered. Each of these proteins play a specific agonistic and/or antagonistic action in the progressive stages of bone callus formation (Kloen et al. 2002; Pazzaglia et al. 1988). Their potential to induce osteogenic cell differentiation has been shown in numerous in vitro and in vivo studies (Heckman et al. 1991; Heckman et al. 1999; Johnson and Urist 1989; Johnson et al. 1990; Reichert et al. 2010). Based on these findings, the two most promising BMPs [BMP-7 (also known as Osteogenic Protein-1, OP-1) and BMP-2] have been produced using recombinant DNA technology for clinical application (Ozkaynak et al. 1990). They have been approved by the FDA for use in human spinal fusion, oral-maxillofacial applications and the treatment of certain fractures (De Biase and Capanna 2005; Friedlaender et al. 2001; Govender et al. 2002).

Nevertheless, the use of these commercially available BMP products is limited, due to the suboptimal delivery system (collagen type I matrix as a carrier), a short protein half-life with difficult dosage control and the need for very high, supraphysiological concentrations of BMP. These high dosages of BMP have resulted in high costs for the clinical application and are not without associated complications (Garrison et al. 2007; Shields et al. 2006).

In the light of these aforementioned limitations associated with current BMP delivery systems and to move towards lowering the dosage and related costs of BMP delivery, several different delivery vehicles have been developed. For the regeneration of segmental long bone defects, a hybrid nanofiber mesh/hydrogel delivery system has been developed to provide spatiotemporal control of protein delivery (Boerckel et al. 2011; Kolambkar et al. 2011). The investigators used the nanofiber mesh tube, in combination with alginate hydrogels and different BMP concentrations, to evaluate the release profile of the alginate hydrogel and ascertain the effect of protein dose on BMP-mediated bone regeneration. The nanofiber mesh tubes served as a barrier retaining the alginate and the delivered BMPs within the bone defect, thereby promoting mineralized matrix formation, preventing extra-anatomical mineralization and serving to target and guide bone formation within the anatomical site (Boerckel et al. 2011; Kolambkar et al. 2011). However, a large amount of residual alginate was still present in the defect 3 months after implantation, which may impede remodelling and restoration of native architecture. Therefore, in this current study we utilized platelet-rich plasma (PRP) instead of alginate. PRP is a concentrated source of autologous platelets and thus may be used as an autologous fibrin glue system. In humans, PRP has been investigated for several types of treatments, including nerve injury, tendonitis, myocardial injury, orthopedics and dentistry (Hildner et al. 2011; Lee et al. 2011).

In order to increase the proliferative and osteoconductive properties of the nanofiber mesh tubes, mineralizing the mesh with a layer of apatite coating is considered to be a promising approach. Comprehensive in vitro and in vivo studies have demonstrated the positive influence of biomimetic apatite coating on the proliferative and osteoconductive properties of PLGA scaffolds (Davies et al. 2010). A comprehensive review was compiled by Kretlow and Mikos (Kretlow and Mikos 2007).

Taking into account these variations to the nanofiber tubes, we therefore investigated the use of CaP-coated nanofiber mesh tube-mediated delivery of BMP-7 from a PRP matrix for the regeneration of critical-sized segmental bone defects in a small animal model.

Material and methods

Fabrication of nanofiber meshes

Nanofiber meshes were produced using electrospinning and formed into cylindrical tubes as described previously (Boerckel et al. 2011; Kolambkar et al. 2011; Oest et al. 2007). Briefly, poly-(ε-caprolactone) (PCL) was dissolved at a concentration of 12% (w/v) in a 90:10 volume ratio of hexaflouro-2-propanol:dimethylformamide (Sigma-Aldrich) and electro-spun onto a static collector. Twenty-four 1-mm diameter perforations were patterned into the nanofiber mesh sheets, which were then glued into tubes of 4.5 mm diameter and 12 mm length. The nanofiber meshes were immersed in ethanol for 30 min under vacuum and then placed into a 2 M natrium hydroxide (NaOH) solution preheated at 37°C in a water bath. A 5-min vacuum treatment was performed in order to facilitate the solution penetration in the depth of the mesh and therefore the efficacy of the alkaline etching. After 30 min at 37°C, the meshes were rinsed five times with ultra-pure water until a neutral pH was reached. Mineralisation of the meshes by a layer of calcium phosphate was performed through exposure to

simulated body fluid (SBF) prepared according to Yang et al. (Yang et al. 2008), with the exception that the pH was adjusted to 6 to increase the solution stability and to delay calcium phosphate precipitation in the solution. Yang et al. showed that using a 10× SBF resulted in the formation of a mixture of nano-apatite and di-calcium phosphate dehydrate. Therefore, it was expected that the coating formed in this present study should be of the same nature, as our experimental conditions did not show any significant differences. SBF solution was filtered with 0.2 μm filters before immersing the meshes. A further 5-min vacuum treatment was then performed to enable infiltration of the SBF solution into the mesh. Thereafter, the meshes were placed at 37°C for 2.5 h, with SBF refreshed every 30 min. A 0.5 M NaOH post-treatment for 30 min at 37°C was performed in order to obtain a homogenous calcium phosphate phase. The meshes were then rinsed five times in ultra-pure water, air dried for 4 h and sterilized by using UV light for 1 h. The surface coating was visualized using scanning electron microscopy (SEM) and microCT (Fig. 1). Nanofiber meshes were kept in sterile tubes in a dessicator until use.

Loading of growth factors to nanofiber meshes

Sterile pulverized bone morphogenetic protein-7 (BMP-7, Stryker®, USA) was used in this experiment. 5 μg of BMP-7 was reconstituted in 120 μl of platelet-rich plasma (PRP) and activated with 60 μl of thrombin (200 U/ml). To produce PRP, 10 ml of blood was collected from donor rats not included in this experiment. The blood was collected in 3.5-ml monovettes, supplemented with sodium citrate (3.8%) and then transferred to falcon tubes and centrifuged for 20 min at 2.400 rpm. Subsequently, the yellow plasma of the tube was transferred to another 15-ml falcon tube and platelets pelleted in a second centrifugation step for 10 min at 3,600 rpm (Weibrich et al. 2001). The pellet was resuspended in 0.3 ml of plasma and the platelets counted in a Neugebauer counting chamber. After preparation, PRP was mixed with the BMP-7, activated by adding thrombin (200U/ml) and then loaded onto the sterilized nanofiber mesh tubes. The PRP layer on the surface of the meshes was visualized using SEM (Fig. 2). The nanofiber meshes were placed in an incubator at 37°C for at least 1 hour before implantation into the defect.

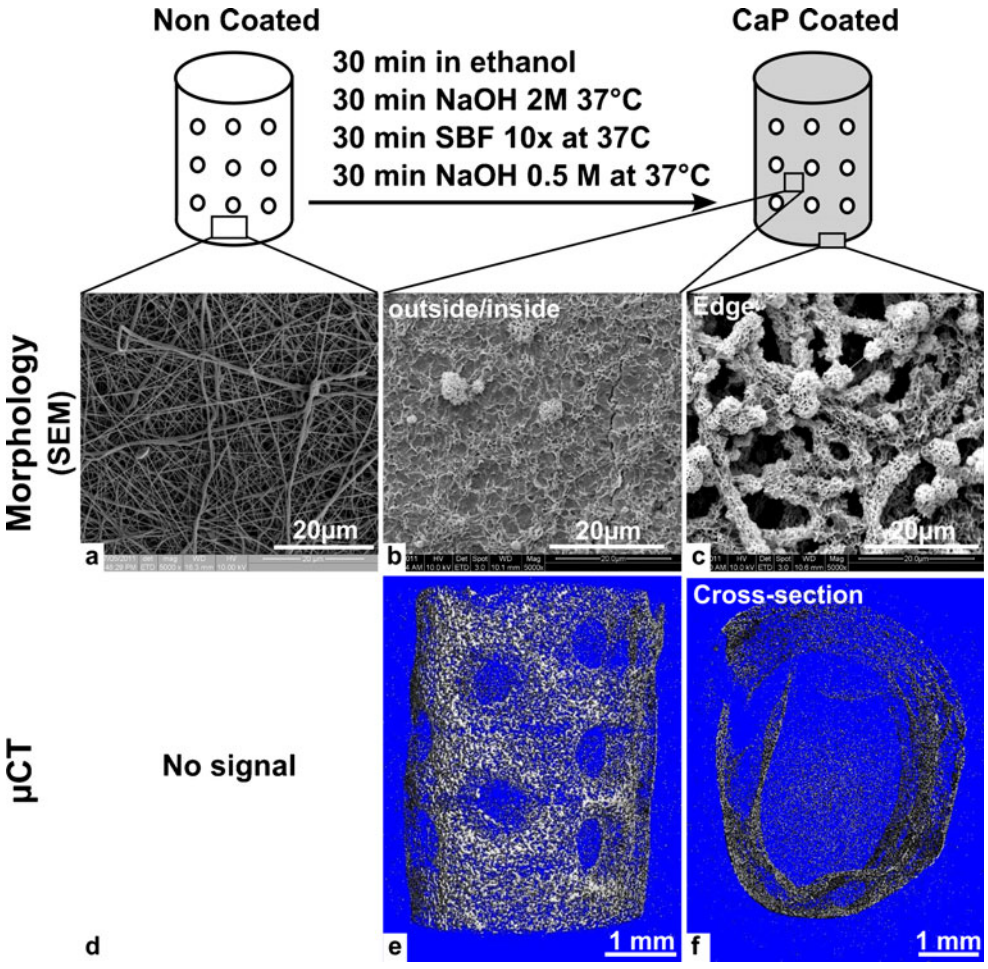

Fig. 1 For uncoated meshes, the individual fibres could be identified using SEM (**a**). After coating of the nanofiber meshes, a homogenous calcium phosphate layer was visualised on the surface using SEM (**b**/**c**). MicroCT scanning revealed the overall mineralisation on the surface (**e**) and across the meshes (**f**) on the coated meshes, whereas no signal was detected on the non-coated meshes (**d**)

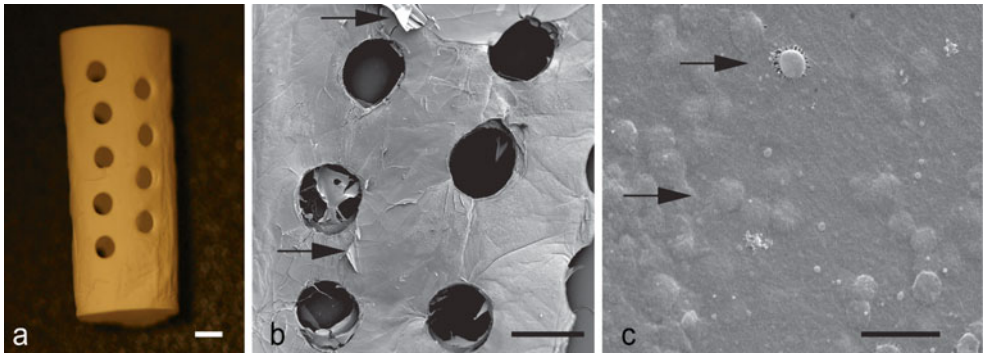

Fig. 2 The nanofiber mesh tubes (**a**; *bar*=1 mm) were loaded with 5 μg BMP-7 in combination with PRP. Due to the freeze-drying processing for SEM, the PRP layer flaked off in several areas (**b**; *arrows* indicate flakes, *bar*=1 mm). Higher magnification shows the homogenous PRP layer on the mesh surface, with several thrombocytes connected with small fibrin fibres (**c**; *arrows* indicate thrombocytes, *bar*=5 μm)

Surgical procedure/experimental groups

Twelve skeletally mature male Lewis rats with a mean bodyweight of 306 g (STDV 25 g) were obtained from Animal Resources Centre, Canning Vale, WA, USA. The rats were housed at the QUT Medical Engineering Research Facility (MERF) at the Prince Charles Hospital, Chermside. The animals received water and pelleted ration ad libitum throughout the experiment. All procedures were approved by the animal ethics committee of the Queensland University of Technology. All rats were operated under general anaesthesia, administered through intraperitoneal injection of a mixture of ketamine and xylazine (75-100 mg/kg ketamine +5-10 mg/kg xylazine). Buprenorphine (0.01–0.05 mg/kg subcutaneously) was used for analgesia preoperatively and post-operatively every 6–12 hours for 3 days. Using an anterior approach, bilateral incisions were made over the length of the femurs (Fig. 3a). Prior to defect creation, the femora were stabilized by modular fixation plates consisting of a polysulfone plate and two stainless steel plates (J.I. Morris Co., Southbridge, MA, USA) (Fig. 3b/c). Bilateral full-thickness diaphyseal segmental defects (8 mm long) were created using a miniature oscillating saw and flushed with saline (Fig. 3d/f) (Oest et al. 2007). Nanofiber mesh tubes were placed around the adjacent bone ends such that the tube lumen contained the defect and there was an overlap of 2.5 mm with the native bone ends at each end of the tube (Fig. 3f). Defects received treatment either with uncoated nanofiber mesh tubes (n=6), CaP-coated nanofiber mesh tubes (n=6; mesh-coated group), CaP-coated nanofiber mesh tubes with PRP (n=6) or CaP-coated nanofiber mesh tubes with BMP-7 (5 μg) and PRP (n=6; BMP group). Furthermore, six femora of unoperated rats from the same breed served as a control group for microCT analysis and biomechanical testing (n=6; control group). The groups were assigned to the right and left limbs to evenly distribute pairs of groups and obtain a balanced experimental design. During anaesthesia, surgery and immediate post-operative period, the rats were kept on a heating pad and after that, they were transferred to a clean warmed cage for recovery. After surgery, the animals were allowed to recover and move freely. Animals were kept for 12 weeks after surgery and then sacrificed by CO_2 inhalation. To collect the implants, the skin was dissected, both femora of the rats were removed and wrapped in phosphate buffered saline (PBS)-soaked gauze and frozen at −20°C until further analysis.

Radiographic and microcomputed tomography analysis (microCT)

After 12 weeks, planar radiographs of the femora were taken in two orientations to qualitatively assess bone regeneration and bridging of the defect. For quantitative evaluation of bone formation, the bones were scanned in a microcomputed tomography scanner (microCT 40, Scanco Medical, Brüttisellen, Switzerland) at an energy of 55 kVp and intensity of 145 μA with 200 ms integration time. For further processing, a threshold of 313.5 mg HA/ccm and a Gauss filter with a filter width of 0.8 and filter support of 1.0 was applied to the scans. X-ray attenuation was correlated to sample density using a standard curve generated by scanning hydroxyapatite phantoms with known mineral densities. Mineralized matrix volume and bone volume fraction were quantified throughout the entire construct and presented as bone volume in mm^3. In addition, the polar moment of inertia (pMOI) in mm^4 was calculated for the defect zone. The pMOI represents a quantity used to predict an object's ability to resist torsion. Six femora of non-operated rats with the same bodyweight served as control values for bone volume and polar moment of inertia.

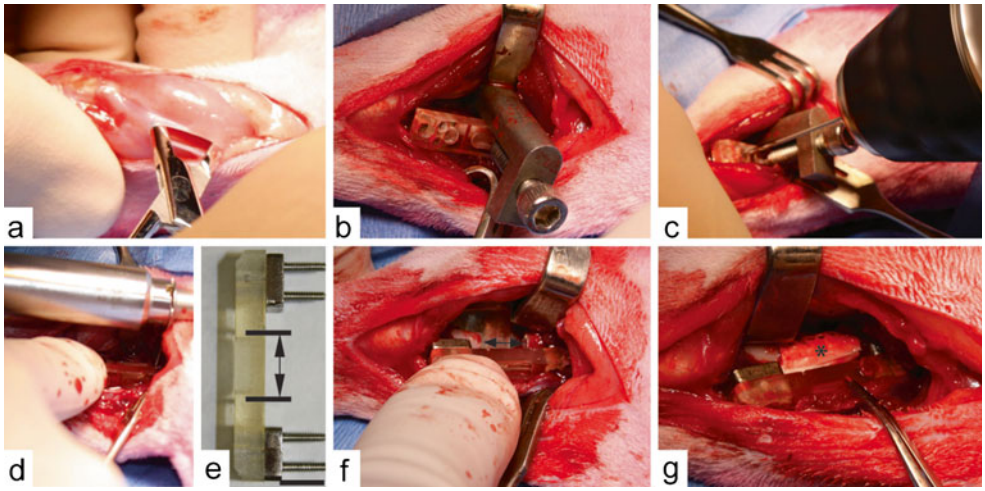

Fig. 3 The skin incision was made antero-lateral at the femur. After cutting through the fat pad, a blunt dissection of the vastus lateralis of the quadriceps was performed (**a**). After exposing the bone, the prepared plate (**e**; *arrow* indicates defect size of 0.8 cm, *bar*=0.5 cm) was inserted and fixed with the holder (**b**). The holes were carefully drilled, beginning with the most proximal followed by the most distal hole (**c**). After sawing the 8-mm segmental defect (**d**), the bone piece was removed and the soft-tissue protector inserted (**f**; *arrow* indicates segmental bone defect). The mesh tubes were carefully inserted with covering the host bone on both sides (**g**; *asterisk* indicates nanofiber mesh tube)

Biomechanical testing

After thawing, the bone ends were carefully cleaned of soft tissue and embedded in plastic cups using polymethylmethacrylate (PMMA) (Paladur, Heraeus Kulzer, Germany). Throughout the preparation, embedding and testing, the bones were kept moist by wrapping them in phosphate buffered saline (PBS) soaked gauze. The embedded bones were then inserted into a custom designed torsion testing set-up for an Instron 5848 Microtester (Instron, Norwood, MA, USA). One end of the bone was fixed, while the other end rotated at 0.58°/s, while torsion angle and torque were recorded. Each bone was tested three times to 2° rotation to determine torsional stiffness and then once until failure to determine torsional strength. Both femora from each animal were tested, with the testing orientation changed for the two bones to ensure testing them in internal rotation, similar to physiological loading. Outcome parameters were calculated in terms of absolute values (torsional stiffness in Nmm/degree, ultimate torque in Nmm) and in percentages for treated bones compared to the six non-operated rat femora, which served as intact control bones.

Histological analysis

For processing decalcified samples into paraffin, the femora were fixed in 10% neutral buffered formalin for 24 h and decalcified in 15% EDTA for 3 weeks at 4°C. The samples were then serially dehydrated in ethanol in a tissue processor (Excelsior ES, Thermo Scientific, Franklin, MA, USA) and embedded in paraffin. Sections (5 μm) were taken using a microtome (Leica RM 2265). The slides were then deparaffinized with xylene and rehydrated with serial concentrations of ethanol, before being stained with haematoxylin and eosin (Sigma-Aldrich) and mounted with Eukitt mountant (Fluka Biochemica, Milwaukee, WI, USA). Selected femora were excised and fixed in 10% neutral buffered formalin for 24 h and changed to 70% ethanol prior to embedding in hard resin (methylmethacrylate, MMA, Sigma Aldrich) to assess the specimens in their non-decalcified state. Longitudinal sections were cut to a thickness of 6 μm using a Leica SL2500 Sledge Microtome and were stained using von Kossa–MacNeal's tetrachrome to identify new bone formation.

Statistics

Statistical analysis was performed for all the quantitative results using Student's *t*-test for comparing means from two independent sample groups. A confidence level of 95% was used ($p<0.05$). All values are displayed as mean values with standard deviation of means.

Results

After 12 weeks, all animals were euthanized and both femora were removed for further evaluations. Macroscopic evaluation of the femurs showed a good integration of the nanofiber mesh tubes to the bone and the surrounding tissues (Fig. 4a). The groups treated with the CaP-coated nanofiber mesh tubes with PRP and the uncoated nanofiber

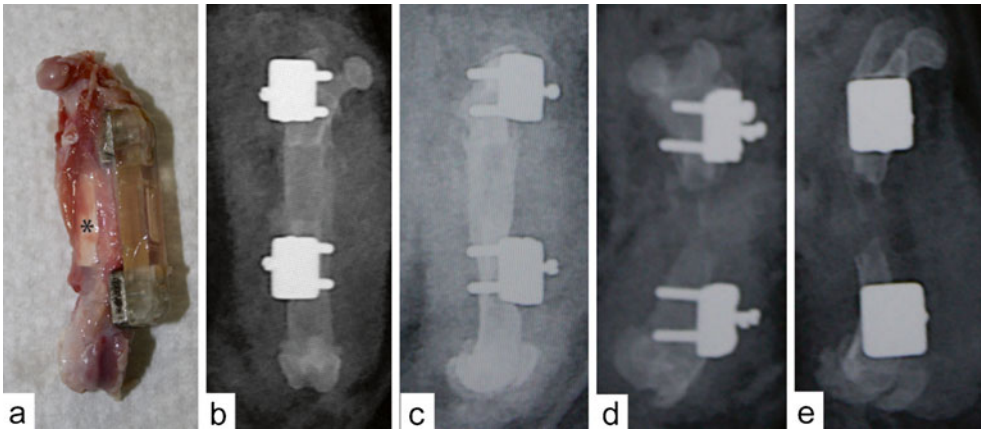

Fig. 4 The nanofiber mesh tubes showed a good integration into the defect site and the surrounding tissues (**a**). Representative X-ray images in two planes, of the BMP-group (**b**/**c**) and the coated mesh group (**d**/**e**) after 12 weeks. Complete bone regeneration and defect bridging could be observed in the BMP group, whereas just a small amount of bone regeneration without defect bridging occurred in the mesh group

mesh tubes did not show any significant differences in the microCT and biomechanical analysis compared to the CaP-coated mesh tubes without PRP (mesh-coated group). Hence, the data of these two groups are not shown.

Radiographic analysis

The radiographs of the defect region showed a complete bridging of the defect, with bone regeneration throughout the defect, for all samples in the BMP group after 12 weeks (Fig. 4b/c). The mineral density of the regenerated tissue appeared lower compared to the adjacent host bone. In the mesh-coated group, no bridging of the defects was seen in any animal up to 12 weeks (Fig. 4d/e), although small amounts of regenerated bone tissue were detected growing from the proximal and distal host bone ends.

microCT analysis

The results of the qualitative evaluation of the bridging of the defects using three-dimensional rendering of the processed microCT were consistent with those of the two-dimensional radiographic analysis (Fig. 5a/b). A significantly higher volume of newly formed bone was found in the BMP-group compared to the mesh-coated group (Fig. 5d). Comparison values for bone volume and polar moment of inertia from unoperated control femora showed slightly more bone volume compared to the BMP-group (not

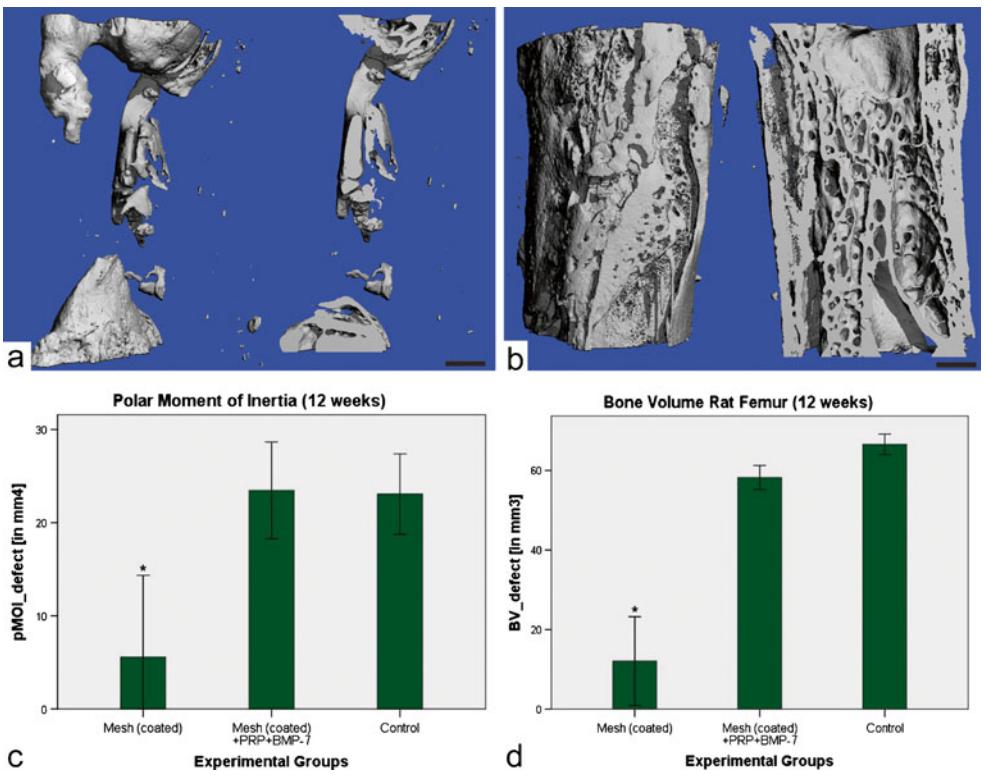

Fig. 5 Representative 3D microCT reconstructions of the complete defect zone from the mesh (coated) group (**a**; *bar*= 1 mm) and the BMP group (**b**; *bar*=1 mm). Bone regeneration was observed throughout the defect in the BMP group (**b**), whereas the mesh (coated) group showed just a small amount of regenerated bone within the defect (**a**). Values for the polar moment of inertia showed the same trend as the results for bone volume (**c**). Bone volume calculations showed significantly more bone formed in the BMP group than in the mesh (coated) group (**d**). *Asterisks* indicate statistical significance. Six femora of non-operated rats served as control values

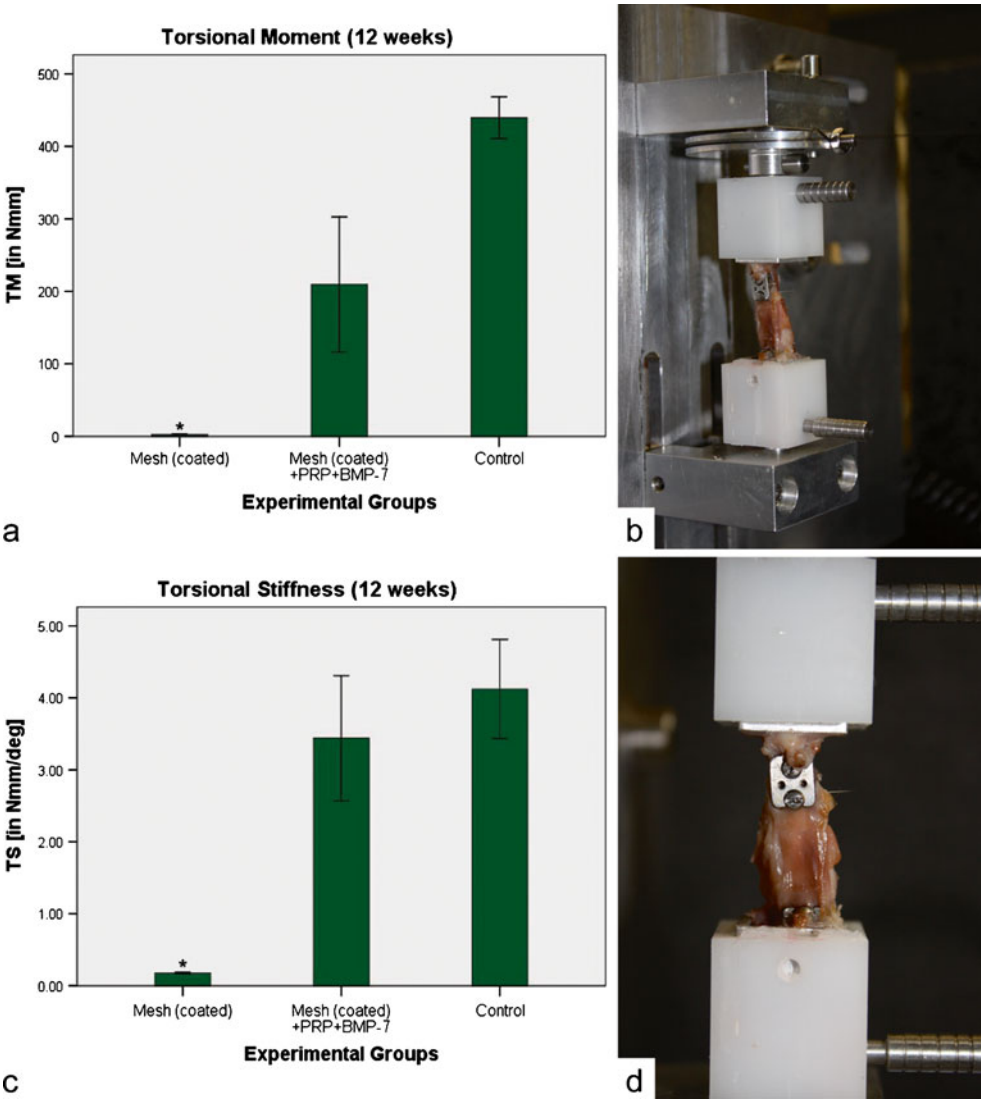

Fig. 6 Biomechanical testing of the maximum torque at failure (**a**) and torsional stiffness (**c**) of the experimental groups in relation to unoperated controls (n=6 per group). The femora were embedded in plastic moulds and the plate for stabilizing the defect was removed before testing (**b**/**d**). *Asterisks* indicate statistical significance

significant). The results for the polar moment of inertia predicted a better mechanical integrity of the bones of the BMP group than the mesh-coated group, whereas no significant difference to the unoperated control femora could be determined (Fig. 5c).

Biomechanical testing

Biomechanical properties of the regenerated femurs were obtained from torsional testing at 12 weeks and compared to control femurs from animals of the same breed and age, not undergoing surgical procedures. The maximum torque at failure of the BMP group was not significantly different from intact controls, though the mean failure torque was approximately 50–60% of the control values (Fig. 6a). The maximum torque values of the mesh coated group were significantly lower than both the BMP group and intact controls, at 5% of the control group, reflecting the poor bridging results from the radiographic analysis. Both the BMP group and intact controls were significantly higher than the mesh coated group (Fig. 6a). The torsional stiffness of the BMP group was not significantly different from intact controls and both were significantly greater than the mesh-coated group (Fig. 6c).

Histology

Histological examinations of decalcified samples were performed after 12 weeks. Representative H&E staining demonstrated clear defect bridging within the BMP group (Fig. 7a, c, d), whereas the mesh-coated group showed just a small formation of new bone tissue (Fig. 7b, e, f). The overview images of the longitudinal sections demonstrate the whole defect site with the adjacent host bone (Fig. 7a/b). The nanofiber mesh tubes showed, in both groups, a good integration to the host bone and can be clearly visualised in pale pink surrounding the dark pink host bone in the H/E

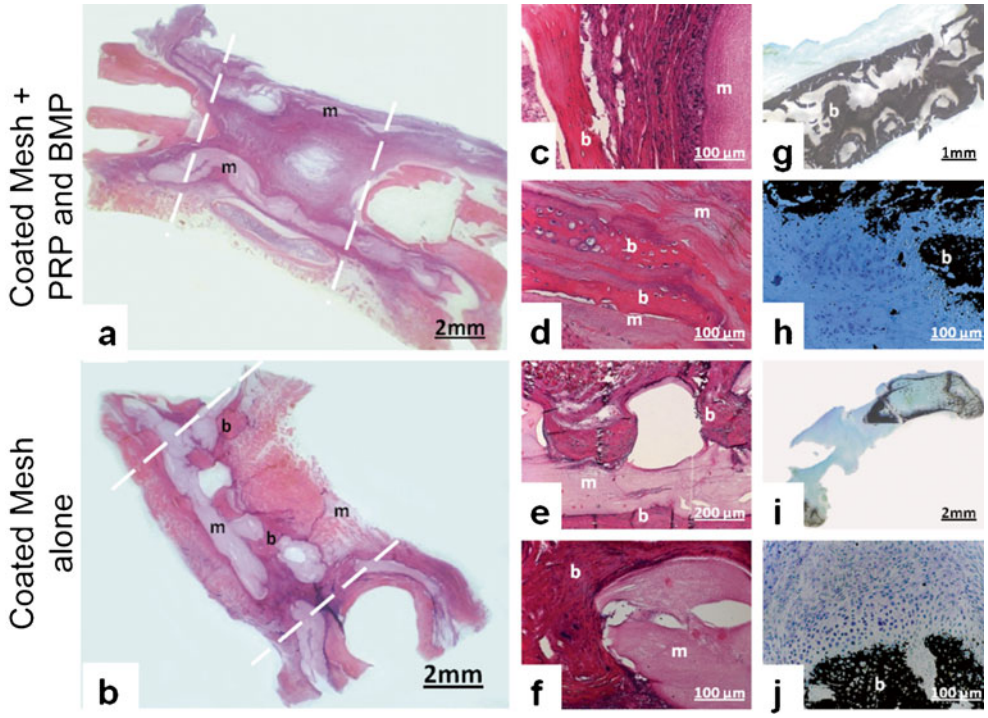

Fig. 7 Histological assessment of the CaP-coated mesh tubes and the CaP-coated mesh tubes with BMP and PRP. H&E staining was performed on longitudinal sections through the entire defect showing the 8-mm defect site with the adjacent host bone and the mesh (**a**/**b**). Bone regeneration can be observed in the BMP group using H&E staining (**a**,**c**,**d**) where the mesh is still visible (*pale pink* labelled "*m*") with adjacent mineralised bone tissue with embedded osteoblasts (osteocytes) labelled "*b*" that indicates new bone formation. Von Kossa–MacNeal's staining (**g**,**h**) shows clear black areas that correspond to mineralised tissue. A high level of mineralisation can be seen throughout the BMP group (**g**), which shows an overview of the defect area. There is also evidence of cartilage tissue formation (**c**), which is commonly a precursor tissue during endochondral ossification and is subsequently mineralised to form bone. A small area of mineralisation at the proximal and distal ends of the coated mesh group can be observed (**i**,**j**). *Dashed lines* indicate defect site and are placed over the image to indicate the edge of the host bone (*dark pink*)

overview images (Fig. 7a/b). In both groups, the newly formed bone tissue was located within the mesh tubes.

Undecalcified resin sections were stained with von Kossa–MacNeal's staining to identify new mineral deposition. The BMP group showed a higher mineralisation within the defect compared to the mesh-coated group (Fig. 7g-j). These results reflect our microCT evaluation and demonstrate some regenerated bone tissue growing from the proximal and distal host bone ends in the case of the coated mesh alone (Fig. 7i), which mirrored the observations from the X-ray. Supplementary Figure 1 depicts a histological assessment of an uncoated mesh tube without PRP or BMP to demonstrate the fact that the coating was playing a role in the bone regeneration, as the uncoated meshes predominantly were filled with fibrous tissue with limited bone formation.

Discussion

In the present study, we used a challenging rat femoral segmental defect model, developed by the Guldberg lab to evaluate bone tissue engineering strategies. We investigated the osteogenic effects of calcium phosphate CaP-coated nanofiber mesh tube-mediated delivery of BMP-7 from a PRP matrix. Together, these data demonstrate the capacity of PRP to act as a delivery vehicle for recombinant proteins and the efficacy of BMP-7 to induce bone regeneration.

The ongoing need for scaffolds in bone engineering is driven by several factors. Firstly there is a surgical requirement to either augment or, alternatively, to avoid reliance upon traditional autograft procedures, which are common practice in orthopedic surgery but are frequently limited by insufficient tissue availability. Secondly there is a need to address the shortcomings of existing materials that may show limited degradation in vivo, an architecture that does not reflect that of the natural tissue, or a porosity and interconnected macroporosity that limits host tissue invasion and sustainable vascularization. Next to the requisite structural properties of the scaffold, the advent of tissue engineering strategies to increase their effectiveness by the incorporation of cells and/or growth factors adds further versatility to the design concept. Biologically active molecules, such as growth factors,need to be added at the physiological temperature or below, since a

higher processing temperature may cause denaturation. Our strategy to develop scaffold-based bone engineering has involved the fabrication of an electrospun tubular construct, which was then surface-modified and had the addition of growth factors via PRP administration.

Given the appositional nature of bone formation, the scaffold surface remains fundamental in bone tissue engineering strategies. The surface modification of the nanofiber mesh tubes with CaP coating demonstrated morphological changes detected by SEM and microCT. The effects of surface modification with calcium phosphate have received mixed reviews in the literature. Some research groups show positive effects of these coatings on bone regeneration and the mechanical properties of the coated biomaterials (Liu et al. 2011), whereas others show no beneficial effects of the coating with respect to bone regeneration (Ekholm et al. 2005; Fontana et al. 2011). It should be noted, however, that most of the defects treated in the aforementioned studies were small bone defects (not critical-sized, thereby able to heal unassisted) or were studies to demonstrate the effects of surface modification on implant ingrowth (Fontana et al. 2011; Mihalko et al. 2010).

Our results show that the mesh-coated group didn't show any bridging of the defect or a large amount of bone formation, although some bone formation was evident. Also, when compared to the uncoated mesh group (Supplementary Figure 1), there was more fibrous tissue within the defect site when the nanofiber mesh was uncoated and very little mineralisation was observed. CaP may abrogate the putative foreign body giant cell response to the underlying polymer, while the internal CaP phase provides dimensional stability. Therefore, we conclude that the surface modification might be helpful to support bone regeneration but the osteogenic potency of the hydroxyapatite coating alone is not strong enough to initiate bone regeneration in a critical-sized segmental bone defect.

"Platelet-rich plasma" (PRP) was first used in the 1990s as a pool of autogenous growth factors for bone regeneration and there are now numerous studies showing the effect of PRP on bone regeneration. However, a recent review concluded that the supportive efficacy of PRP can be considered controversial (Redler et al. 2011); many studies were able to demonstrate a positive effect, whereas others could not. PRP does not exhibit any significant immunogenicity, therefore it can be used in allogenic and xenogenic transplantation. In our study, we choose pooled allogenic PRP to assure that the PRP was uniform and homogenous and that variations caused by inhomogeneous PRP could be avoided. Nonetheless, numerous authors prefer autogenous PRP and described it to be more potent. Our results in the present study should be considered against this background.

These data demonstrate that platelet-rich plasma delivery of BMP-7 within a nanofiber mesh tube resulted in robust bone formation and complete bridging of the defects with new bone. With this treatment, the bone volume and polar moment of inertia were not significantly different from uninjured controls, indicating full defect regeneration. Likewise, indicators of functional restoration, torsional stiffness and maximum torque at failure were not significantly different from intact age-matched limbs, though the maximum torque of the BMP group was approximately 60% of that of controls. Taken together with the volumetric microCT data, this suggests that the material strength of the newly formed bone is lower than that of intact bone, probably due to the presence of woven bone, which has an inherently lower fracture toughness than lamellar cortical bone (Weiner and Wagner 1998). However, it can be hypothesized that the woven bone would continue to remodel over time and that the final outcome would be a fully regenerated defect with lamellar bone architecture.

Overall, these biomechanical, radiological and histological results show that a CaP-coated tubular nanofiber mesh loaded with PRP/BMP-7 is able to regenerate a large segmental defect. Future studies have to be designed for up to at least 6 months, to show that the woven bone formation detected after 3 months, is completely remodelled into lamellar bone.

Acknowledgements This work was supported by funding through the Australian Research Council and the German Research Foundation (DFG)(BE 4492/1-2). We thank Stryker for providing the BMP-7.

References

Boerckel JD, Kolambkar YM, Dupont KM, Uhrig BA, Phelps EA, Stevens HY, Garcia AJ, Guldberg RE (2011) Effects of protein dose and delivery system on BMP-mediated bone regeneration. Biomaterials 32:5241–5251

Davies JE, Matta R, Mendes VC, Perri de Carvalho PS (2010) Development, characterization and clinical use of a biodegradable composite scaffold for bone engineering in oro-maxillo-facial surgery. Organogenesis 6:161–166

De Biase P, Capanna R (2005) Clinical applications of BMPs. Injury 36(Suppl 3):S43–S46

Ekholm E, Tommila M, Forsback AP, Martson M, Holmbom J, Aaritalo V, Finnberg C, Kuusilehto A, Salonen J, Yli-Urpo A et al (2005) Hydroxyapatite coating of cellulose sponge does not improve its osteogenic potency in rat bone. Acta Biomater 1:535–544

Fontana F, Rocchietta I, Addis A, Schupbach P, Zanotti G, Simion M (2011) Effects of a calcium phosphate coating on the osseointegration of endosseous implants in a rabbit model. Clin Oral Implants Res 22:760–766

Friedlaender GE, Perry CR, Cole JD, Cook SD, Cierny G, Muschler GF, Zych GA, Calhoun JH, LaForte AJ, Yin S (2001) Osteogenic protein-1 (bone morphogenetic protein-7) in the treatment of tibial nonunions. J Bone Joint Surg Am 83(Suppl 1):S151–S158

Garrison KR, Donell S, Ryder J, Shemilt I, Mugford M, Harvey I, Song F (2007). Clinical effectiveness and cost-effectiveness of bone morphogenetic proteins in the non-healing of fractures and

spinal fusion: a systematic review. Health Technol Assess 11:1–150, iii–iv

Govender S, Csimma C, Genant HK, Valentin-Opran A, Amit Y, Arbel R, Aro H, Atar D, Bishay M, Borner MG et al (2002) Recombinant human bone morphogenetic protein-2 for treatment of open tibial fractures: a prospective, controlled, randomized study of four hundred and fifty patients. J Bone Joint Surg Am 84:2123–2134

Heckman JD, Boyan BD, Aufdemorte TB, Abbott JT (1991) The use of bone morphogenetic protein in the treatment of non-union in a canine model. J Bone Joint Surg Am 73:750–764

Heckman JD, Ehler W, Brooks BP, Aufdemorte TB, Lohmann CH, Morgan T, Boyan BD (1999) Bone morphogenetic protein but not transforming growth factor-beta enhances bone formation in canine diaphyseal nonunions implanted with a biodegradable composite polymer. J Bone Joint Surg Am 81:1717–1729

Hildner F, Albrecht C, Gabriel C, Redl H, van Griensven M (2011) State of the art and future perspectives of articular cartilage regeneration: a focus on adipose-derived stem cells and platelet-derived products. J Tissue Eng Regen Med 5:e36–e51

Johnson EE, Urist MR (1989) Distal metaphyseal tibial nonunions associated with significant bowing deformity and cortical bone loss: treatment with human bone morphogenetic protein (h-BMP) and internal fixation. Nippon Seikeigeka Gakkai Zasshi 63:613–620

Johnson EE, Urist MR, Finerman GA (1990). Distal metaphyseal tibial nonunion. Deformity and bone loss treated by open reduction, internal fixation, and human bone morphogenetic protein (hBMP). Clin Orthop Relat Res :234-240

Kloen P, Doty SB, Gordon E, Rubel IF, Goumans MJ, Helfet DL (2002) Expression and activation of the BMP-signaling components in human fracture nonunions. J Bone Joint Surg Am 84:1909–1918

Kolambkar YM, Dupont KM, Boerckel JD, Huebsch N, Mooney DJ, Hutmacher DW, Guldberg RE (2011) An alginate-based hybrid system for growth factor delivery in the functional repair of large bone defects. Biomaterials 32:65–74

Kretlow JD, Mikos AG (2007) Review: mineralization of synthetic polymer scaffolds for bone tissue engineering. Tissue Eng 13:927–938

Lee KS, Wilson JJ, Rabago DP, Baer GS, Jacobson JA, Borrero CG (2011) Musculoskeletal applications of platelet-rich plasma: fad or future? AJR Am J Roentgenol 196:628–636

Liu W, Yeh YC, Lipner J, Xie J, Sung HW, Thomopoulos S, Xia Y (2011) Enhancing the stiffness of electrospun nanofiber scaffolds with a controlled surface coating and mineralization. Langmuir 27 (15):9088–9093

Mihalko WM, Howard C, Dimaano F, Dimaano N, Hawkins M (2010) Effects of hydroxyapatite on titanium foam as a bone ingrowth surface in acetabular shells: a canine study. J Long Term Eff Med Implants 20:35–42

Oest ME, Dupont KM, Kong HJ, Mooney DJ, Guldberg RE (2007) Quantitative assessment of scaffold and growth factor-mediated repair of critically sized bone defects. J Orthop Res 25:941–950

Ozkaynak E, Rueger DC, Drier EA, Corbett C, Ridge RJ, Sampath TK, Oppermann H (1990) OP-1 cDNA encodes an osteogenic protein in the TGF-beta family. EMBO J 9:2085–2093

Pazzaglia UE, Zatti G, Ragni P, Ceciliani L (1988) The role of mineralization in experimental models of osteogenetic induction with decalcified bone matrix. Ital J Orthop Traumatol 14:369–375

Perry CR (1999) Bone repair techniques, bone graft, and bone graft substitutes. Clin Orthop Relat Res 360:71-86

Redler LH, Thompson SA, Hsu SH, Ahmad CS, Levine WN (2011) Platelet-rich plasma therapy: a systematic literature review and evidence for clinical use. Phys Sportsmed 39:42–51

Reichert JC, Woodruff MA, Friis T, Quent VM, Gronthos S, Duda GN, Schutz MA, Hutmacher DW (2010) Ovine bone- and marrow-derived progenitor cells and their potential for scaffold-based bone tissue engineering applications in vitro and in vivo. J Tissue Eng Regen Med 4:565–576

Shields LB, Raque GH, Glassman SD, Campbell M, Vitaz T, Harpring J, Shields CB (2006) Adverse effects associated with high-dose recombinant human bone morphogenetic protein-2 use in anterior cervical spine fusion. Spine (Phila Pa 1976) 31:542–547

Urist MR (1965) Bone: formation by autoinduction. Science 150:893–899

Weibrich G, Kleis WK, Kunz-Kostomanolakis M, Loos AH, Wagner W (2001) Correlation of platelet concentration in platelet-rich plasma to the extraction method, age, sex, and platelet count of the donor. Int J Oral Maxillofac Implants 16:693–699

Weiner S, Wagner HD (1998) The material bone: structure mechanical function relations. Annu Rev Mater Sci 28:271–298

Xiao C, Zhou H, Liu G, Zhang P, Fu Y, Gu P, Hou H, Tang T, Fan X (2011) Bone marrow stromal cells with a combined expression of BMP-2 and VEGF-165 enhanced bone regeneration. Biomed Mater 6:015013

Yang F, Wolke JGC, Jansen JA (2008) Biomimetic calcium phosphate coating on electrospun poly (epsilon-caprolactone) scaffolds for bone tissue engineering. Chem Eng J 137:154–161